J Therm Spray Tech (2022) 31:1276–1284
https://doi.org/10.1007/s11666-022-01359-3

PEER REVIEWED

Microstructure and High-Temperature Tribological Behavior of Plasma-Sprayed FeCoCrAlNi High Entropy Alloy Coatings Under Higher Load Condition

Xin Liu[1] · Fan Lv[1,2] · Hongwei Li[2] · Yongguang Wang[1] · Xiaolong Lu[1] · Dong Zhao[1]

Submitted: 16 September 2021 / in revised form: 18 January 2022 / Accepted: 3 February 2022 / Published online: 2 March 2022

Abstract In this study, FeCoCrAlNi high entropy alloy (HEA) anti-wear coating was prepared on 304 stainless steel by plasma spraying. The results show that the HEA powder and coating phase is mainly the BCC phase. The microstructure of the splat exhibits a disk shape without obvious splashes, and the coating presents a dense microstructure with a typical lamellar structure. The average microhardness of the coating is 411 $HV_{1.0}$ which is almost 1.5 times that of the 304 stainless steel substrate. Compared with the substrate, the HEA coating exhibits a better wear resistance property under a high load (20 N) at room temperature and 800 °C. The wear mechanisms for the FeCoCrAlNi coating were oxidation wear and mild abrasive wear at room temperature, and mild abrasive wear, oxidation wear, adhesive wear and the formation of oxide films at high temperature. These results indicate that HEA can be a promising high-temperature anti-wear coating material under severe working conditions.

Keywords high entropy alloy · plasma spraying · tribological properties

Introduction

304 stainless steel has been widely used in mechanical, medical, nuclear engineering, and chemical applications due to its good mechanical properties, corrosion resistance, and high cost-effectiveness. However, its poor tribological properties and decreasing mechanical properties at elevated temperatures restrict its applications as key tribological moving components under severe working conditions, such as high temperature, heavy load, oxidation or high-temperature corrosion (Ref 1-3). As the breakdown of tribological moving components owing to wear occurs mainly from their surfaces, fabricating a protective coating on its surface can be an optimum choice. In general, surface engineering techniques for preparing anti-wear coatings include thermal spraying technology (Ref 4-7), physical vapor deposition (Ref 8, 9) and laser cladding (Ref 10, 11). Due to its scalability, versatility, and rapid processing, plasma spraying has been recognized as a cost-effective surface engineering technique to deposit a wide range of materials (metals, ceramics, cermets, intermetallics, and their composites) on a variety of substrate materials to improve the lifespan of solid materials under the above-mentioned severe working conditions (Ref 22).

High entropy alloys (HEAs) generally include five or more major metallic elements in equimolar or near-equimolar proportions. Under the influence of the high entropy effect, HEAs tend to form simple solid-solution

This article is part of a special topical focus in the Journal of Thermal Spray Technology on High Entropy Alloy and Bulk Metallic Glass Coatings. The issue was organized by Dr. Andrew S.M. Ang, Swinburne University of Technology; Prof. B.S. Murty, Indian Institute of Technology Hyderabad; Distinguished Prof. Jien-Wei Yeh, National Tsing Hua University; Prof. Paul Munroe, University of New South Wales; Distinguished Prof. Christopher C. Berndt, Swinburne University of Technology. The issue organizers were mentored by Emeritus Prof. S. Ranganathan, Indian Institute of Sciences.

✉ Xiaolong Lu
shannonlu@126.com

✉ Dong Zhao
zhaodong@suda.edu.cn

[1] School of Mechanical and Electrical Engineering, Soochow University, Suzhou 215021, China

[2] School of Iron and Steel, Soochow University, Suzhou 215021, China

phases instead of intermetallic compounds and produce solid solution hardening, which is an essential strengthening mechanism (Ref 12, 13). In addition, according to the Gibbs rule, multi-component alloys have higher entropies so that each component could contribute its properties (Ref 14, 15). These special effects make HEAs possess multiple superior properties, such as high strength, high ductility, excellent corrosion resistance, radiation resistance, and wear resistance (Ref 16-19). To make full use of the superior properties of HEAs, it is an effective method to fabricate HEA coatings by plasma spraying (Ref 20, 21). Meghwal et al. (Ref 22) reported that AlCoCrFeNi HEA coatings exhibited excellent wear resistance at 500 °C compared to room temperature, which was mainly ascribed to the wear mechanism changes from a combination of delamination wear and adhesive wear at room temperature to oxidative and abrasive wear at elevated temperature. Li et al. (Ref 23) found that the $FeCoCrNiMo_{0.2}$ HEA coatings exhibited good wear resistance due to the self-lubricating behavior of oxide film formation. Löbel et al. (Ref 24) reported that AlCoCrFeNiTi HEA coating with BCC phase can possess a high microhardness of 730 ± 82 $HV_{0.1}$ and a higher wear resistance at room temperature. Nevertheless, very few studies have comprehensively evaluated the tribological properties of HEA coatings, including the coefficient of friction, wear debris, worn surface of the HEA coating, and running-in surface of the counter-body, especially for the wear test under the high temperature and heavy load. In addition, the plasma spraying coating is constructed by the accumulation of individual splats layer by layer, so the microstructure of the splats significantly influences their functional properties. Unfortunately, the splat characterization of HEAs has rarely been reported in the previous literature.

In the present study, FeCoCrAlNi HEA anti-wear coating was fabricated on 304 stainless steel by plasma spraying. The splat morphology and the microstructure, phase and microhardness of the coating were investigated systematically. Dry sliding wear tests were conducted on the coating and substrate using a Al_2O_3 ball with a high load (20 N) at room temperature and 800 °C. The tribological properties were investigated and elucidated through the worn surface of the 304 stainless steel, FeCoCrAlNi HEA coating, counter-body Al_2O_3 ball, and wear debris. This study explores the potential applications of HEA coatings to improve the lifespan of high-temperature key tribological moving components such as rolling/sliding bearing and gears used in the aerospace and automobile industries.

Experimental Section

FeCoCrAlNi HEA powder with spherical shapes was purchased from Jiangsu Vilory Advanced Materials Tech Co., Ltd., China. The powder shows good sphericity and smooth surface, contributing to good flowability for plasma spraying (Fig. 1a). In addition, the particle size distribution was measured using a Mastersizer 2000 instrument (Malvern, the UK). FeCoCrAlNi HEA powder shows a range from 50 to 100 μm with Dv50 = 76.50 μm, and the distribution of particle size is presented in Fig. 1b. Before plasma spray, 304 stainless steel substates (100 × 10 × 3 mm) were blasted with Al_2O_3 particles with an average size of ~1 mm and cleaned with alcohol. HEA coating was fabricated using a SG 100 gun (Praxair Surface Technology, Danbury, CT) on a stainless steel substrate. The details of the plasma spray parameters were as follows: arc voltage 40 V, current 800 A, spray distance 80 mm, power carrier gas (argon) flow rate 8 slpm, primary gas (argon) flow rate 36 slpm, and second gas (helium) flow rate 38 slpm.

The Vickers hardness (HV) was tested on the coating and substrate at least ten times with a load of 10 N and a

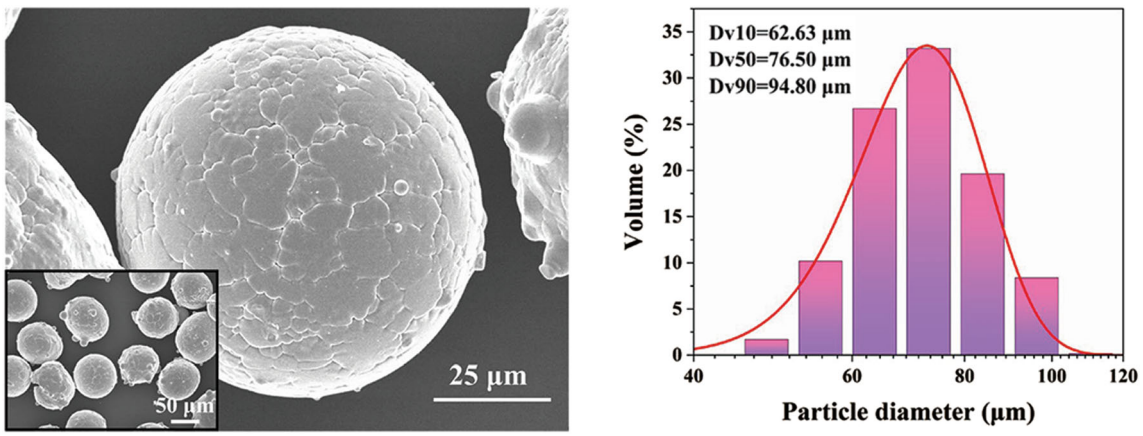

Fig. 1 (a) SEM images of the FeCoCrAlNi HEA powders and (b) the distribution of particle size

dwell time of 10 s using a microhardness tester (HXD-1000 TMC, Shanghai Taiming Optical Instrument Co., Ltd., China). The tribological behaviors were conducted using an HT-1000 tribometer (Lanzhou Zhongkekaihua Science and Technology Co., Ltd., China) with a ball-on-disk mode. The Al_2O_3 ceramic ball with a diameter of 4 mm was used as the counter-body. The wear tests were performed on each sample at least three times at room temperature and 800 °C for 30 min with a high applied load of 20 N, a rotation radius of 2 mm, and a linear velocity of 3.768 m/min. The contact pressure (p) at the beginning of the wear test is calculated by the Hertz model (Ref 25):

$$p = \frac{3F}{2\pi a^2} = \frac{1}{\pi}\left(\frac{6FE^{*2}}{R^2}\right)^{1/3} \quad \text{(Eq 1)}$$

$$\frac{1}{E^*} = \frac{1-v_1^2}{E_1} + \frac{1-v_2^2}{E_2} \quad \text{(Eq 2)}$$

where F is the applied load of 20 N, R is the radius of the Al_2O_3 ball, E^* is the effective modulus, E_1 (320 GPa) and E_2 are the elastic modulus, and v_1 (0.22) and v_2 (0.3) are the Poisson's ratios of the Al_2O_3 ball and coating/substrate, respectively. Nanoindentation tests were conducted on ten different regions of the coating and 304 stainless steel substrate using an MCT tester (CSM, Switzerland) with a diamond spherical indenter under a maximum load of 1000 mN, loading/unloading rate of 2000 mN/min, and dwell time of 10 s. The elastic modulus of the coating and 304 stainless steel was computed for approximately 139 and 227 GPa. Therefore, the estimated contact pressure p at the beginning of the test is approximately 2.2 GPa for the coating and 2.7 GPa for the substrate. After the wear test, the wear volumes of the coating and substrate were measured by the surface mapping profiler of the tribometer. The wear rates were calculated by:

$$W = \frac{V}{LS} \quad \text{(Eq 1)}$$

in which W is the wear rate, V is the wear volume, S is the sliding distance, and L is the applied load.

The interlayer information of the powder and coating was measured by x-ray diffraction (XRD, Ultima IV) at 40 mA and 40 kV. The morphology of splat morphology,

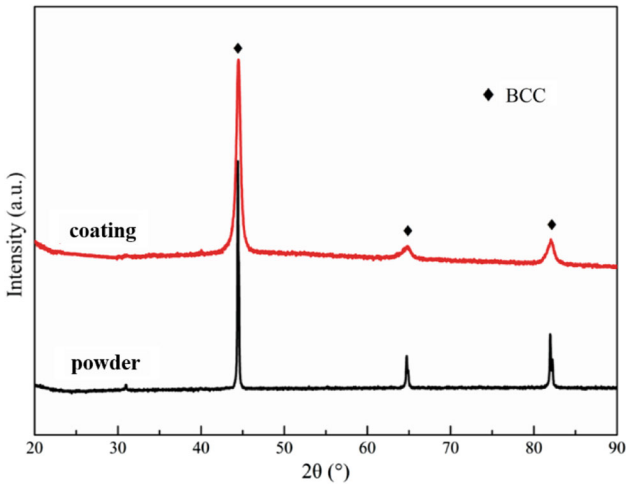

Fig. 2 XRD patterns of the FeCoCrAlNi HEA powder and coating

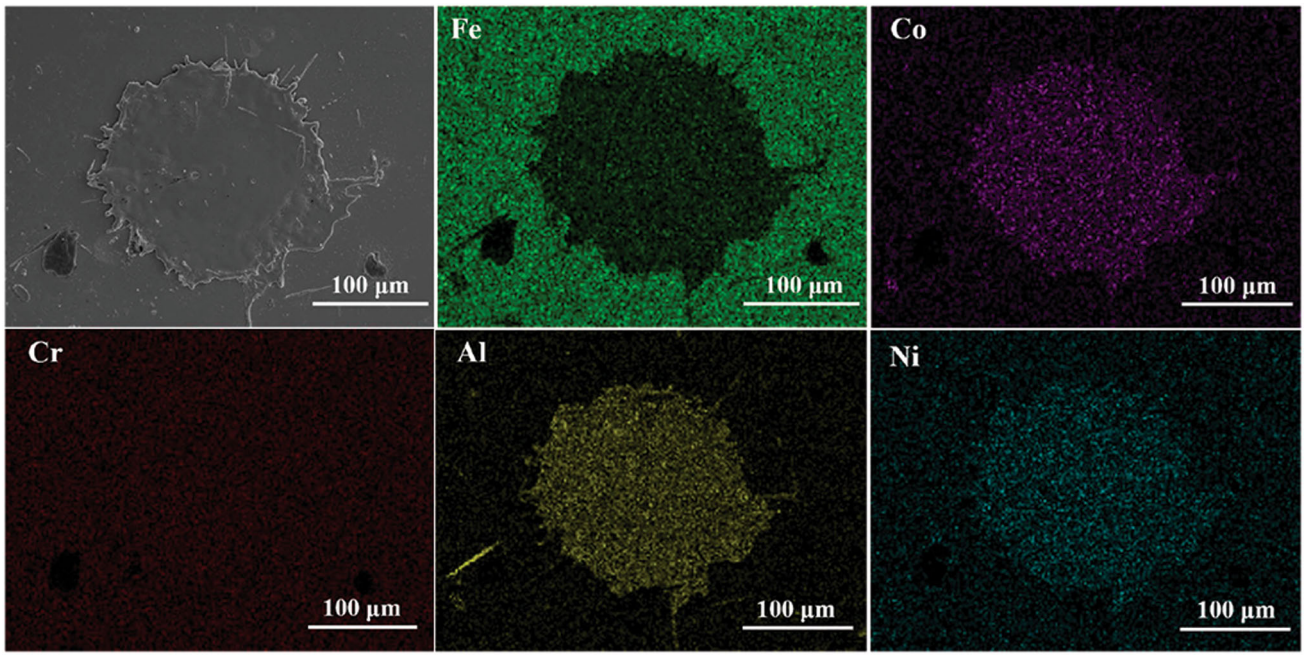

Fig. 3 SEM images of the splat for FeCoCrAlNi HEA powder and corresponding EDS elemental mapping

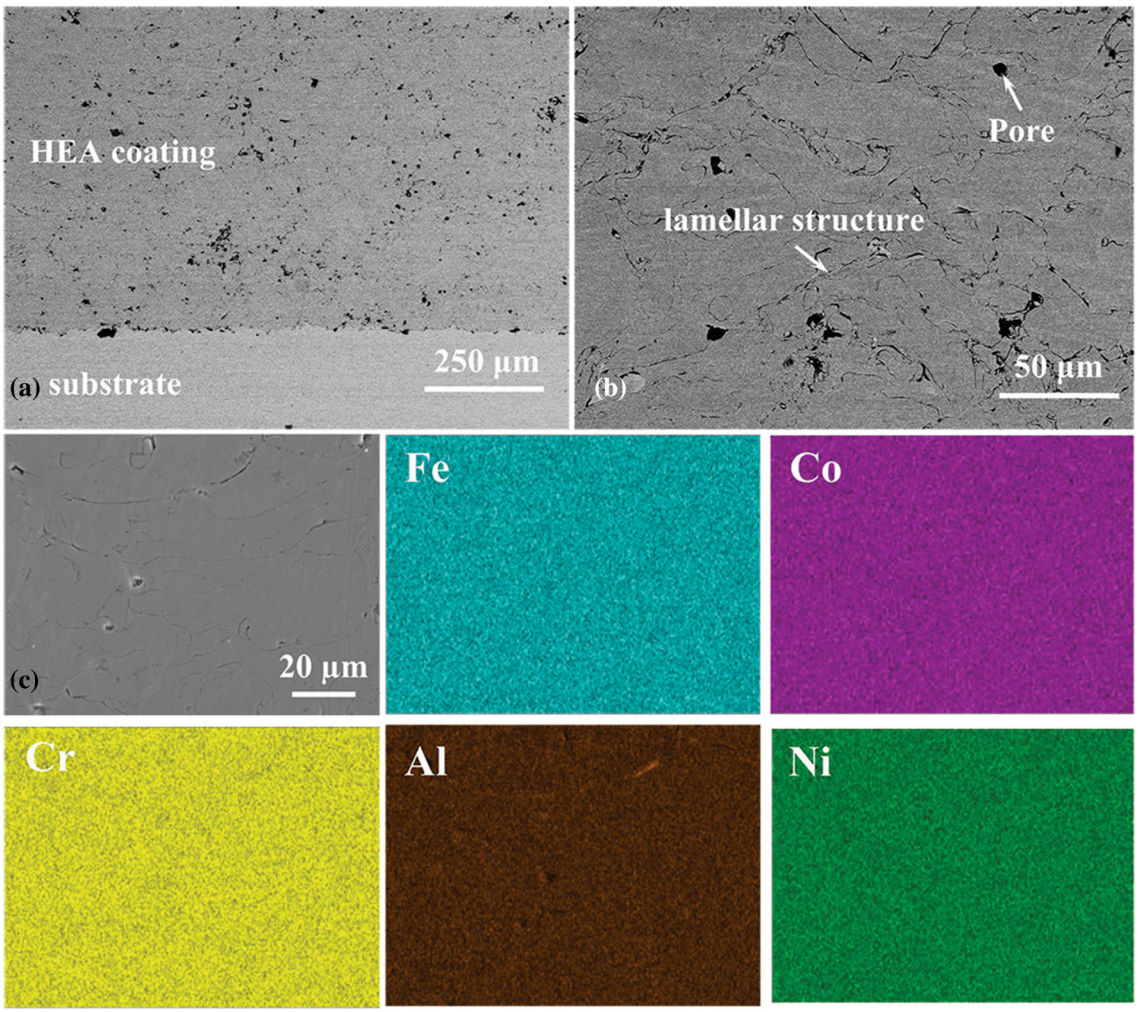

Fig. 4 (a, b) BSE cross-sectional images of FeCoCrAlNi HEA coating, and (c) EDS elemental mapping

the cross-sectional microstructure of as-sprayed coating, and the wear traces of coating, stainless steel substrate and Al_2O_3 balls were performed using a scanning electron microscope (SEM, Hitachi S-4700, Japan) associated with an energy-dispersive x-ray analyzer (EDS).

Results and discussion

Figure 2 shows the XRD patterns of the FeCoCrAlNi HEA powder and coating. The FeCoCrAlNi powders exhibit a typical single-phase body-centered-cubic (BCC) structure. The peaks of the coating are almost the same as those of the raw powder, indicating that there is no change in the phase structure after the plasma spraying process. Furthermore, no peaks of oxides can be identified, demonstrating that the content of oxides is very low. It is worth mentioning that the XRD peak of the coating widens after plasma spraying. Such broadened peaks in coatings are attributed to the high-energy impact of particles onto the substrate during the process of plasma spraying, leading to the formation of coatings with a small crystallite size and poor crystallinity (Ref 26, 27).

When the FeCoCrAlNi HEA feedstock passed through the plasma jet, the HEA particles were melted to form a droplet. Then, the droplet would impact the substrate and flatten out to form a splat by rapid solidification. Figure 3 shows a SEM image of the FeCoCrAlNi HEA splat. It is observed that the individual splat apparently exhibits a disk shape with a diameter of approximately 190 μm and without an obvious splash. The corresponding EDS mapping of Al, Co, Fe and Ni is uniformly distributed in the splat (the distribution of Cr cannot be identified due to the stainless steel 304 substate containing a certain amount of Cr). The deposition behavior of the individual splats can directly affect the coating microstructure (Ref 28, 29), which will be discussed in the sections below.

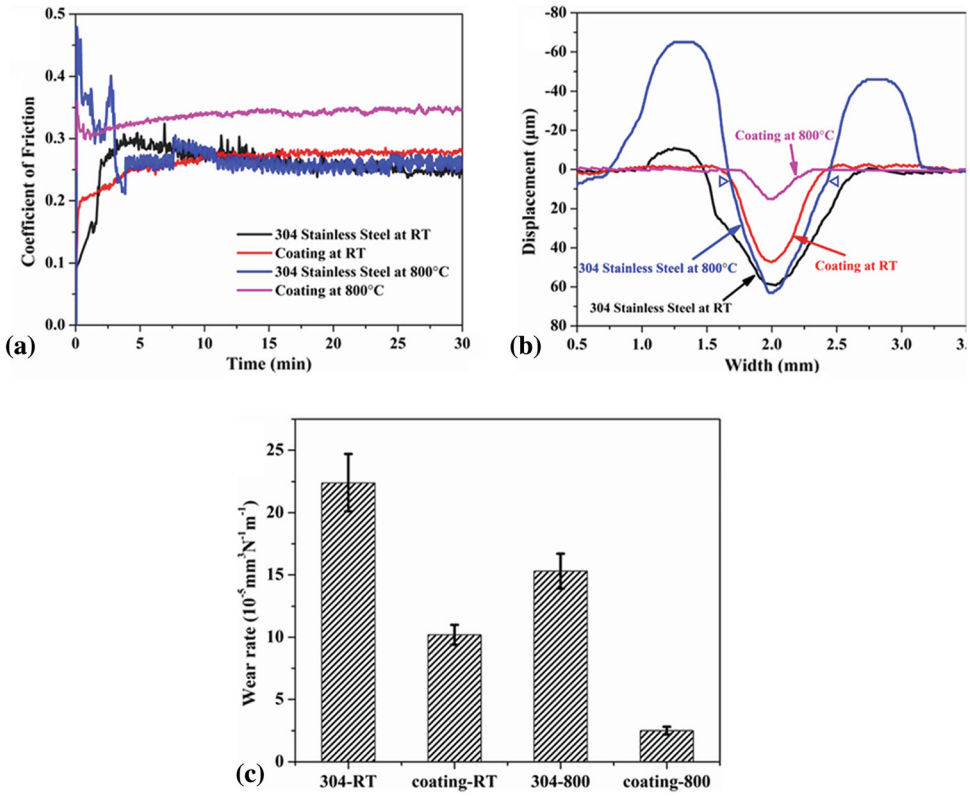

Fig. 5 Coefficient of friction (a), surface profiles across the wear surfaces (b) and wear rate (c) of the 304 stainless steel substrate and FeCoCrAlNi HEA coating at room temperature and 800 °C

Figure 4a, b shows the BSE cross-sectional morphologies of the FeCoCrAlNi HEA coating, which present a dense microstructure with a typical lamellar structure owing to the layer-by-layer stacking of splats. During the plasma spraying process, these HEA powders could be fully melted to form droplets that subsequently rapidly impact, flatten and solidify on the previously deposited splat surface to form the HEA coating. Some small pores (the average porosity of the coating calculated was 4.0 ± 0.5%) can be seen owing to the high surface tension, which prevents liquid splats from completely filling crevices in the substrate. The corresponding EDS mapping of Al, Co, Fe and Ni is uniformly distributed in the coating, and there is no element enrichment region (Fig. 4c). Different from the previous literature results (Ref 30, 31), our coating does not have color-different phases, such as black, white and gray phases, and these color-different phases were called the enrichment areas of different elements. This may be due to our coating elements being homogeneously distributed, which can be seen from EDS mappings of individual splats and can also be evidenced by the XRD results. The average microhardness of the coating is ~ 411 $HV_{1.0}$, which is approximated to bulk HEA materials (Ref 32-34) and higher than that of the substrate ~ 267 $HV_{1.0}$. In addition, it has been reported that BCC-structured HEAs can exhibit better mechanical properties, including high strength, hardness and wear resistance, than FCC-structured HEA (Ref 14, 35, 36). Therefore, it can be deduced that plasma spraying can fabricate a dense HEA coating with a BCC structure, which is expected to have excellent tribological properties close to bulk HEA materials.

Figure 5 shows the coefficient of friction and surface profiles across the worn surfaces of the substrate and coating. It can be seen from Fig. 5a that the coefficient of friction of the coating (0.27 ± 0.01 for room temperature and 0.34 ± 0.01 for 800 °C) is higher than that of the substrate (0.26 ± 0.02 for room temperature and 0.26 ± 0.03 for 800 °C). However, the coefficients of friction for the coating fluctuate more smoothly than those of the substrate at room temperature and 800 °C. Furthermore, Fig. 5b, c suggest that the coating presents excellent wear resistance properties at room temperature and 800 °C, and the wear rates of the coating at room temperature (10.2 ± 0.8 × 10^{-5} mm^3/m N) and 800 °C (2.5 ± 0.3×10^{-5} mm^3/m N) are much lower than those of the substrate, which are 22.4 ± 2.3 × 10^{-5} mm^3/m N at room temperature and 15.3 ± 1.4 × 10^{-5} mm^3/m N at 800 °C.

The worn surface of the substrate at room temperature shows obvious plowing grooves (Fig. 6a), and wear debris are mainly powders and flake-like chips (Fig. 6b). Moreover, the worn surface of the counterpart of the Al_2O_3 ball shows a coarse surface owing to the brittle fracture of the Al_2O_3 ceramic during the wear test, which can be observed

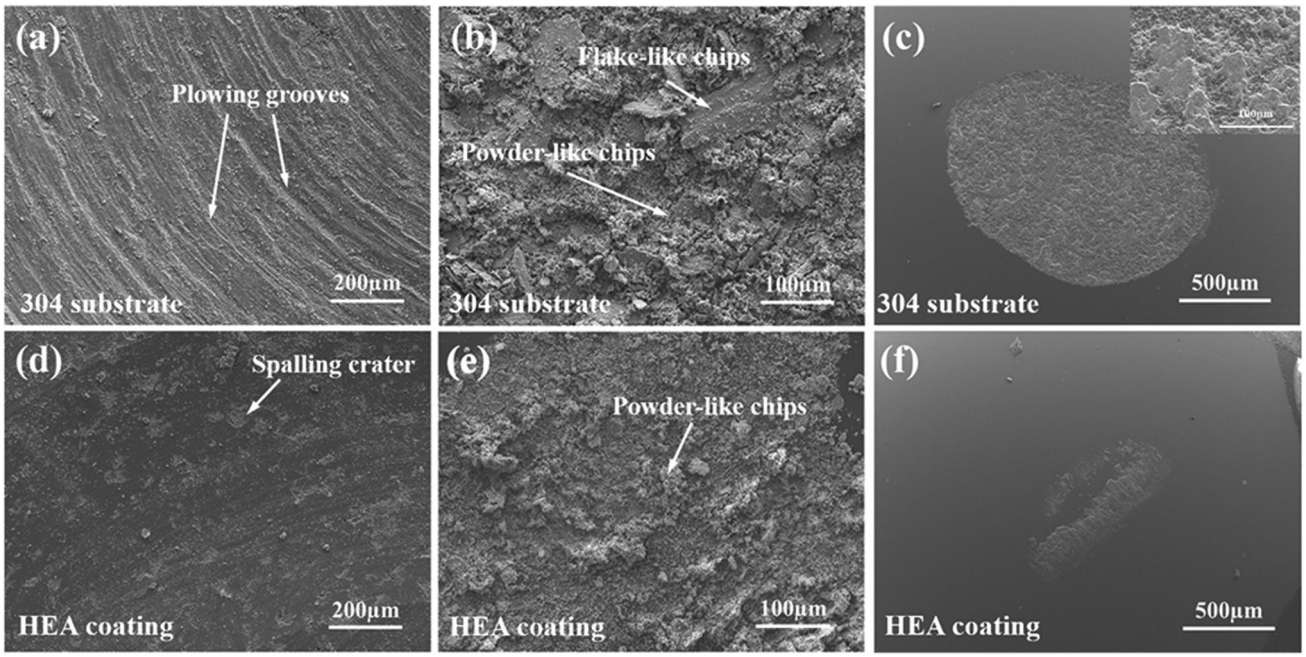

Fig. 6 SEM images of worn surfaces (a, d), wear debris (b, e) and worn surfaces for the counter-body Al_2O_3 balls (c, f) of the 304 stainless steel substrate and FeCoCrAlNi HEA coating at room temperature

from the inset image in Fig. 6c. Figure 5b indicates that the effective contact area of the substrate is higher than that of the coating, leading to the higher worn surface of the counter-body Al_2O_3 ball. Meanwhile, amounts of flake-like wear debris with large size coming from the substrate due to plowing from the substrate by the Al_2O_3 ball cause severe three-body abrasive wear and adhesive wear, resulting in a drastic fluctuation in the coefficient of friction. An instantaneous high friction force would occur, owing to the unstable friction force, and lead to high lateral stress that introduces wear damage to the worn surface of the substrate and the Al_2O_3 ball. Hence, the drastic fluctuation of the coefficient of friction would have an adverse effect (brittle fracture) on the running-in surface of the Al_2O_3 ball.

Compared with the substrate, the HEA coating has a smooth worn surface with a partially spalling crater (Fig. 6d) and powder-like wear debris (Fig. 6e). The size of the worn surface for the counter-body Al_2O_3 ball against the coating in Fig. 6f is also much smaller than that against the substrate. These results suggest that the coating with excellent wear resistance property is beneficial to the running-in surface of the counter-body ball during the wear test at room temperature. In addition, the HEA coating with higher microhardness and better wear resistance can obtain a smaller effective contact area (Fig. 5b) and wear damage to the Al_2O_3 ball. The powder-like wear debris from the coating can be oxidized more easily during the wear test, as shown in Table 1 (32.8 at.% for wear debris of HEA coating and 20.8 at.% for wear debris of 304 stainless steel), resulting in the formation and maintenance of oxide films and protecting the coating from being damaged by the Al_2O_3 ball (Ref 37) and lower fluctuation of the coefficient of friction. The wear mechanism of the coating at room temperature could be mainly oxidation wear and mild abrasive wear.

Table 1 EDS analysis of the worn surface and wear debris in Fig. 6 and 7

Area	EDS quantitative results (at.%)					
	Fe	Co	Cr	Al	Ni	O
Figure 6a	60.0	…	17.6	1.8	5.9	14.8
Figure 6b	54.0	…	15.9	4.1	5.2	20.8
Figure 6d	18.3	18.8	18.9	17.4	17.7	9
Figure 6e	14.6	13.6	14.1	11.6	13.2	32.8
Figure 7a	38.6	…	8.7	0.8	3.1	48.8
Figure 7b	39.4	…	7.7	0.8	3.1	49.0
Figure 7d	10.0	8.3	13.9	11.7	8.0	48.2
Figure 7e	12.2	11.2	10.3	8.3	8.4	49.5

Obvious peeling pits on the worn surface of the substrate (Fig. 7a) result in the formation of flake-like chips and powder-like wear debris (Fig. 7b) during the high-temperature wear test, which is due to the decreasing mechanical properties of stainless steel at elevated temperatures (Ref 38, 39). Surface fatigue occurs during the

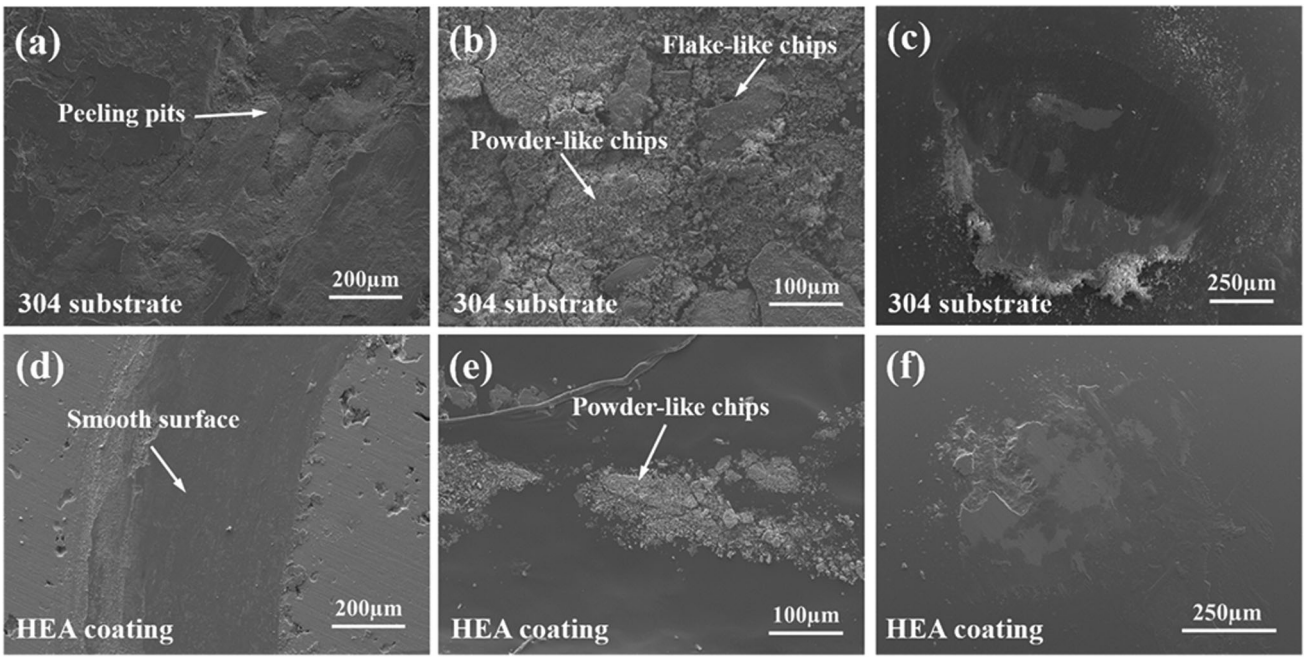

Fig. 7 SEM images of worn surfaces (a, d), wear debris (b, e) and worn surfaces for the counter-body Al_2O_3 balls (c, f) of the 304 stainless steel substrate and FeCoCrAlNi HEA coating at 800 °C

repeated sliding wear test at 800 °C under high load. Repeated loading and unloading cycles to the substrate may induce the formation of subsurface or surface cracks, leading to the breakup of the surface with the formation of flake-like chips (Fig. 7b), leaving large peeling pits after a critical number of cycles. Meanwhile, some flake-like chips would be fractured by a fatigue process during repeated loading and unloading action to form powder-like chips (Fig. 7b). It should be noted that adhesion could also occur at the asperity contacts at the interface, resulting in the detachment of flake-like chips from the substrate and attachment to the Al_2O_3 ball, as shown in Fig. 7c. The large flake-like chips owing to fatigue wear and the occurrence of adhesive wear would cause a higher fluctuation of the coefficient of friction than the coefficient of friction of the substrate at room temperature (Fig. 5a). A higher percentage of O (Table 1) can be detected on the worn surface, and wear debris for the substrate at 800 °C suggests that the substrate could be easily oxidized at high temperature. In addition, the poor mechanical properties of stainless steel at 800 °C and the occurrence of oxidation wear can cause a smaller damaged area to the running-in surface of the Al_2O_3 ball (Fig. 7c). The main wear mechanisms for the substrate are fatigue wear, adhesive wear, three-body abrasive wear, and oxidation wear. Compared with the coefficient of friction of 304 stainless steel at room temperature, the coefficient of friction initially increased and then decreased after some cycles. Since the mechanical properties of 304 stainless steel would decrease at elevated temperature, the initially extremely high contact stress owing to the low effective contact area (ball-on-disk) would cause severe plastic deformation and peeling pits of the substrate, resulting in an increasing friction force and increasing coefficient of friction. After some cycles, the contact stress decreased with increasing contact area, leading to lower wear damage to the worn surface of the substrate. Meanwhile, three-body abrasive wear, adhesive wear and oxidation wear would also decrease the coefficient of friction. It is worth mentioning that the FeCoCrAlNi HEA coating presents an excellent wear resistance performance during the wear test at 800 °C, and the worn surface is much smoother than the coating during the room temperature wear test. Only small amounts of wear debris can be collected and present powder-like morphology. The EDS analysis in Table 1 and wear debris confirm that the wear mechanisms are mainly mild abrasive wear and oxidation wear. Moreover, the oxidation wear could contribute to the formation and maintenance of oxide films which can be directly found on the worn surface of the Al_2O_3 ball from Fig. 7f owing to the adhesive wear. The formation and maintenance of oxide films between the running-in surfaces of the coating and Al_2O_3 ball could protect them from further wear damage during the wear test. However, the adhesive wear also causes a higher lateral sliding force leading to an increased coefficient of friction, as shown in Fig. 5a.

Conclusions

A FeCoCrAlNi high entropy alloy anti-wear coating was prepared on 304 stainless steel by plasma spraying. The splat morphology, microstructure, phase, microhardness, and tribological properties were investigated systematically. This work is expected to explore the potential high-temperature tribological applications of FeCoCrAlNi HEA coatings and encourage the study of more types of HEA coatings in future work. The main conclusions can be drawn as follows:

(1) Plasma spraying can fabricate a dense BCC-structured HEA coating with a microhardness of 542 $HV_{0.2}$ which is almost 1.6 times that of the 304 stainless steel substrate.

(2) Compared with the substrate, the wear rate of the coating at room temperature (10.2×10^{-5} mm^3/m N) and high temperature (2.5×10^{-5} mm^3/m N) significantly decreased by 54 and 84%, respectively. Meanwhile, the coefficient of friction of the coating fluctuates more smoothly at room temperature and high temperature.

(3) The wear mechanisms for 304 stainless steel were severe three-body abrasive wear and adhesive wear at room temperature, and fatigue wear, adhesive wear, three-body abrasive wear, and oxidation wear at high temperature.

(4) The wear mechanisms for the FeCoCrAlNi coating were oxidation wear and mild abrasive wear at room temperature, and mild abrasive wear, oxidation wear, adhesive wear and the formation of oxide films at high temperature. The FeCoCrAlNi coating exhibits excellent wear resistance, suggesting the great potential applications of HEAs as anti-wear coatings working in severe conditions.

Acknowledgments This research work was financially supported by National Natural Science Foundation of China (Grant Numbers: 51501121, 51475315, 51775360, 51701134, 52071124), National Key R&D Program of China (2017YFB1103601), and NSAF (Grant No. U2030102) for financial support.

References

1. J. Chen, R.-M. Asmussen, D. Zagidulin, J.-J. Noël and D.-W. Shoesmith, Electrochemical and Corrosion Behavior of a 304 Stainless-Steel-Based Metal Alloy Wasteform in Dilute Aqueous Environments, *Corros. Sci.*, 2013, **66**, p 142-152.
2. G.-F. Sun, Y.-K. Zhang, M.-K. Zhang, R. Zhou, K. Wang, C.-S. Liu and K.-Y. Luo, Microstructure and Corrosion Characteristics of 304 Stainless Steel Laser-Alloyed with Cr-CrB2, *Appl. Surf. Sci.*, 2014, **295**, p 94-107.
3. J. Xu, X. Wu and E. Han, Acoustic Emission Response of Sensitized 304 Stainless Steel During Intergranular Corrosion and Stress Corrosion Cracking, *Corros. Sci.*, 2013, **73**, p 262-273.
4. X. Liu, X. Lu, Y. Song, S. Xia, R. Ren, Y. Wang, D. Zhao and M. Wang, Plasma-Sprayed Graphene Nanosheets/ZnO/Al2O3 Coatings with Highly Efficient Microwave Absorption Properties, *J. Therm. Spray Techn.*, 2021, **30**, p 1524-1534.
5. X. Lu, S. Bhusal, G. He, D. Zhao, C. Zhang, A. Agarwal and Y. Chen, Efficacy of Graphene Nanoplatelets on Splat Morphology and Microstructure of Plasma Sprayed Alumina Coatings, *Surf. Coat. Technol.*, 2019, **366**, p 54-61.
6. B. Malvi and M. Roy, Elevated Temperature Erosion of Plasma Sprayed Thermal Barrier Coating, *J. Therm. Spray Techn.*, 2021, **30**, p 1028-1037.
7. P. Ctibor, V. Stengl and Z. Pala, Structural and Photocatalytic Characteristics of TiO2 Coatings Produced by Various Thermal Spray Techniques, *Journal of Advanced Ceramics*, 2013, **2**, p 218-226.
8. Y. Deng, W. Chen, B. Li, C. Wang, T. Kuang and Y. Li, Physical Vapor Deposition Technology for Coated Cutting Tools: A Review, *Ceram. Int.*, 2020, **46**, p 18373-18390.
9. L. Baptiste, N.-V. Landschoot, G. Gleijm, J. Priede, J. Schade Van Westrum, H. Velthuis and T. Kim, Electromagnetic Levitation: A New Technology for High Rate Physical Vapour Deposition of Coatings Onto Metallic Strip, *Surf. Coat. Technol.*, 2007, **202**, p 1189-1193.
10. H. Zhang, Y. Pan and Y. He, Synthesis and Characterization of FeCoNiCrCu High-Entropy Alloy Coating by Laser Cladding, *Mater. Des.*, 2011, **32**, p 1910-1915.
11. M.-J. Tobar, C. Álvarez, J.-M. Amado, G. Rodríguez and A. Yáñez, Morphology and Characterization of Laser Clad Composite NiCrBSi-WC Coatings on Stainless Steel, *Surf. Coat. Technol.*, 2006, **200**, p 6313-6317.
12. X.-D. Xu, S. Guo, T.-G. Nieh, C.-T. Liu, A. Hirata and M.-W. Chen, Effects of Mixing Enthalpy and Cooling Rate on Phase Formation of AlxCoCrCuFeNi High-Entropy Alloys, *Materialia*, 2019, **6**, p 100292.
13. Y.-F. Ye, Q. Wang, J. Lu, C.-T. Liu and Y. Yang, High-Entropy Alloy: Challenges and Prospects, *Mater. Today (Kidlington, England)*, 2016, **19**, p 349-362.
14. J. Wu, S. Lin, J. Yeh, S. Chen, Y. Huang and H. Chen, Adhesive Wear Behavior of AlxCoCrCuFeNi High-Entropy Alloys as a Function of Aluminum Content, *Wear*, 2006, **261**, p 513-519.
15. C. Tung, J. Yeh, T. Shun, S. Chen, Y. Huang and H. Chen, On the Elemental Effect of AlCoCrCuFeNi High-Entropy Alloy System, *Mater. Lett.*, 2007, **61**, p 1-5.
16. M. Chuang, M. Tsai, W. Wang, S. Lin and J. Yeh, Microstructure and Wear Behavior of AlxCo1.5CrFeNi1.5Tiy High-Entropy Alloys, *Acta Mater.*, 2011, **59**, p 6308-6317.
17. S. Zhu, Z. Zhang, B. Zhang, Y. Yu, Z. Wang, X. Zhang and B. Lu, Microstructure and Properties of Al2O3-13wt.%TiO2-Reinforced CoCrFeMnNi High-Entropy Alloy Composite Coatings Prepared by Plasma Spraying, *J. Therm. Spray Techn.*, 2021, **30**, p 772-786.
18. H. Liang, H. Yao, D. Qiao, S. Nie, Y. Lu, D. Deng, Z. Cao and T. Wang, Microstructures and Wear Resistance of AlCrFeNi2W0.2Nbx High-Entropy Alloy Coatings Prepared by Laser Cladding, *J. Therm. Spray Techn.*, 2019, **28**, p 1318-1329.
19. S.-A. Firstov, V.-F. Gorban, N.-A. Krapivka, M.-V. Karpets and A.-D. Kostenko, Wear Resistance of High-Entropy Alloys, *Powder Metall. Met. C.*, 2017, **56**, p 158-164.
20. A. Meghwal, A. Anupam, B.-S. Murty, C.-C. Berndt, R.-S. Kottada and A.-S.-M. Ang, Thermal Spray High-Entropy Alloy Coatings: A Review, *J. Therm. Spray Techn.*, 2020, **29**, p 857-893.

21. J. Xiao, T. Li, Y. Wu, J. Chen and C. Zhang, Microstructure and Tribological Properties of Plasma-Sprayed CoCrFeNi-based High-Entropy Alloy Coatings Under Dry and Oil-Lubricated Sliding Conditions, *J. Therm. Spray Techn.*, 2021, **30**, p 926-936.
22. A. Meghwal, A. Anupam, V. Luzin, C. Schulz, C. Hall, B.-S. Murty, R.-S. Kottada, C.-C. Berndt and A.-S.-M. Ang, Multiscale Mechanical Performance and Corrosion Behaviour of Plasma Sprayed AlCoCrFeNi High-Entropy Alloy Coatings, *J. Alloy. Compd.*, 2021, **854**, p 157140.
23. T. Li, Y. Liu, B. Liu, W. Guo and L. Xu, Microstructure and Wear Behavior of FeCoCrNiMo0.2 High Entropy Coatings Prepared by Air Plasma Spray and the High Velocity Oxy-Fuel Spray Processes, *Coatings*, 2017, **7**, p 151.
24. M. Löbel, T. Lindner, T. Mehner and T. Lampke, Microstructure and Wear Resistance of AlCoCrFeNiTi High-Entropy Alloy Coatings Produced by HVOF, *Coatings*, 2017, **7**, p 144.
25. E.-F. Sukur and G. Onal, Graphene Nanoplatelet Modified Basalt/Epoxy Multi-Scale Composites with Improved Tribological Performance, *Wear*, 2020, **460**, p 460-461.
26. S. Singh, V.-K. Meena, M. Sharma and H. Singh, Preparation and Coating of Nano-Ceramic on Orthopaedic Implant Material Using Electrostatic Spray Deposition, *Mater. Des.*, 2015, **88**, p 278-286.
27. B. Hahn, D. Park, J. Choi, J. Ryu, W. Yoon, B. Lee and H. Kim, Effect of the HA/β-TCP Ratio on the Biological Performance of Calcium Phosphate Ceramic Coatings Fabricated by a Room-Temperature Powder Spray in Vacuum, *J. Am. Ceram. Soc.*, 2009, **92**, p 793-799.
28. L. Chen and G. Yang, Epitaxial Growth and Cracking of Highly Tough 7YSZ Splats by Thermal Spray Technology, *J. Adv. Ceram.*, 2018, **7**, p 17-29.
29. L. Tian, J. Wang, Q. Zhang, R. Li and C. Liu, Microstructure Characterization of AlCoCrFeNiTi High-Entropy Alloy Coating Produced by Atmospheric Plasma Spraying, *Mater. Res. Express*, 2019, **6**, p 116416.
30. L. Wang, F. Zhang, S. Yan, G. Yu, J. Chen, J. He and F. Yin, Microstructure Evolution and Mechanical Properties of Atmosphere Plasma Sprayed AlCoCrFeNi High-Entropy Alloy coatings Under Post-Annealing, *J. Alloy. Compd.*, 2021, **872**, p 159607.
31. Y. Mu, L. Zhang, L. Xu, K. Prashanth, N. Zhang, X. Ma, Y. Jia, Y. Xu, Y. Jia and G. Wang, Frictional Wear and Corrosion Behavior of AlCoCrFeNi High-Entropy Alloy Coatings Synthesized by Atmospheric Plasma Spraying, *Entropy-Switz.*, 2020, **22**, p 740.
32. S. Zhang, C.-L. Wu, C.-H. Zhang, M. Guan and J.-Z. Tan, Laser Surface Alloying of FeCoCrAlNi High-Entropy Alloy on 304 Stainless Steel to Enhance Corrosion and Cavitation Erosion Resistance, *Opt. Laser Technol.*, 2016, **84**, p 23-31.
33. Y. Wang, Y. Yang, H. Yang, M. Zhang, S. Ma and J. Qiao, Microstructure and Wear Properties of Nitrided AlCoCrFeNi High-Entropy Alloy, *Mater. Chem. Phys.*, 2018, **210**, p 233-239.
34. Q. Fan, C. Chen, C. Fan, Z. Liu, X. Cai, S. Lin and C. Yang, Effect of High Fe Content on the Microstructure, Mechanical and Corrosion Properties of AlCoCrFeNi High-Entropy Alloy Coatings Prepared by Gas Tungsten Arc Cladding, *Surf. Coat. Technol.*, 2021, **418**, p 127242.
35. J.-W. Yeh, S.-K. Chen, S.-J. Lin, J.-Y. Gan, T.-S. Chin, T.-T. Shun, C.-H. Tsau and S.-Y. Chang, Nanostructured High-Entropy Alloys with Multiple Principal Elements: Novel Alloy Design Concepts and Outcomes, *Adv. Eng. Mater.*, 2004, **6**, p 299-303.
36. Z. Lei, X. Liu, Y. Wu, H. Wang, S. Jiang, S. Wang, X. Hui, Y. Wu, B. Gault, P. Kontis, D. Raabe, L. Gu, Q. Zhang, H. Chen, H. Wang, J. Liu, K. An, Q. Zeng, T. Nieh and Z. Lu, Enhanced Strength and Ductility in a High-Entropy Alloy Via Ordered Oxygen Complexes, *Nature*, 2018, **563**, p 546-550.
37. G.-F. Sun, K. Wang, R. Zhou, Z.-P. Tong and X.-Y. Fang, Effect of Annealing on Microstructure and Mechanical Properties of Laser Deposited Co-285+WC Coatings, *Opt. Laser Technol.*, 2015, **66**, p 98-105.
38. M. Calmunger, G. Chai, R. Eriksson, S. Johansson and J.-J. Moverare, Characterization of Austenitic Stainless Steels Deformed at Elevated Temperature, Metallurgical and materials transactions, *Phys. Metal. Mater. Sci.*, 2017, **48**, p 4525-4538.
39. L. Gardner, A. Insausti, K.-T. Ng and M. Ashraf, Elevated Temperature Material Properties of Stainless Steel Alloys, *J. Constr. Steel Res.*, 2010, **66**, p 634-647.